Combining airborne hyperspectral and LiDAR data across local sites for upscaling shrubland structural information: lessons for HyspIRI

Jessica. J. Mitchell[1*], Rupesh Shrestha[2], Lucas P. Spaete[2], Nancy. F. Glenn[2]

[1]Department of Geography and Planning
Appalachian State University
P.O. Box 32066
Boone, NC 28608, USA.

[2]Boise Center Aerospace Laboratory
Department of Geosciences
Boise State University
1910 University Drive
Boise, ID 83725-1535, USA.

*Corresponding Author:
Jessica J. Mitchell
Tel: 828.262.7054
Email: mitchelljj@appstate.edu

Submitted to HyspIRI Special Issue

Abstract

Fine-scale variation of vegetation structure in dryland systems, such as the Great Basin in the western US, is critical to understanding ecosystem responses to changing land-use conditions. High resolution airborne hyperspectral (HyMap) and LiDAR datasets acquired across independent collection sites can reduce uncertainty in predictive ecosystem modeling and provide a basis for regional upscaling to satellite observations of structural metrics such as cover and height. In the first part of our study, we combined ground reference and airborne data collected at three sagebrush-steppe locations and used the statistical data mining tool random forests to identify remote sensing variables most relevant to estimating shrub cover. In the second part of our study, we hypothesized that vegetation indices derived from hyperspectral satellite observations would not only reliably predict shrub cover but also be relatable to shrub height; thereby augmenting the collection of vertical structure estimates from future satellite platforms such as ICESAT-2. To test this hypothesis, we simulated HyspIRI observations to derive variables to relate to LiDAR-based estimates of shrub cover and height. We generated the same hyperspectral variables as in the first part of this study but at coarser resolution (60m) and we again used random forests to model shrub cover and height and identify predictors of greatest importance. Overall, combining LiDAR and HyMap datasets at the airborne scale improved shrub cover model results (r^2 = 0.58) compared to LiDAR alone (r^2 = 0.49). Primary shrub cover variables of importance were H_{IQR} (the interquartile range of height of all LiDAR vegetation returns), H_{MAD} (Median Absolute Deviation from median height of all LiDAR vegetation returns), a narrowband index sensitive to anthocyanins, the ratio of LiDAR vegetation returns to total returns, and a red to green ratio. In addition, HyspIRI-simulated narrowband vegetation indices were relatable to LiDAR-derived shrub cover and height variables (r^2 ranging from 0.63 to 0.71)

with relatively low root mean square error.

Keywords

LiDAR, hyperspectral, HsypIRI, sagebrush, vegetation structure

1. Introduction

Sagebrush (*Artemisia* spp.) communities once covered approximately 63 million hectares of rangeland in the western United States and Canada and represent the largest and one of the most threatened ecosystems in the temperate semi-desert ecoregion of North America (Anderson & Inouye, 2001; Homer et al., 2012). Sagebrush habitat provides food or cover for over 350 wildlife species including sage grouse (Knick & Connelly, 2009; Suring et al., 2005; Tilley et al., 2006). Like most vegetation, sagebrush cover and height characteristics vary across the landscape. Accurately mapping this variation is important for sage grouse habitat selection, which depends on percent canopy cover, visual cover and height; and for habitat modeling (e.g. Crawford et al., 2004; Krogh et al., 2002). Cover and height are also relevant to estimating fuel loads (e.g. Castedo-Dorado et al., 2012; Keane et al., 2002) and aboveground biomass (Mathieu et al., 2013), which are indicators of forage potential, species dominance and hydrologic function in semiarid systems. When coupled with canopy shape, sagebrush cover and height provide information about the spatial pattern of vegetation roughness, which directly affects aeolian sediment transport (Mueller et al., 2007; Okin, 2008) and may be relatable to aerodynamic roughness, a key parameter in energy balance models and evapotranspiration (Lee et al., 2012) and shrub patch dynamics (Schlesinger et al., 1990). Fine-scale characterization of the variability in sagebrush height and cover is important to initialize terrestrial ecosystem models (e.g. Medvigy et al., 2009) to understand structural dynamics and provide regional estimates of carbon stock and fluxes under future climate change scenarios.

Several studies have demonstrated the use of multispectral imagery (1 m to 56 m pixels) for monitoring categorical and continuous shrub cover change in sagebrush ecosystems (e.g., Ramsey et al., 2004; Sivanpallai et al., 2009; Stow et. al., 2008). However, multispectral and hyperspectral studies designed to estimate vegetation cover in sagebrush are limited by multiple scattering, bright soil reflectance, penetrable canopies and spectrally indiscriminate targets (e.g., Laliberte et al., 2007; Mitchell & Glenn, 2009; Okin et al., 2001; Smith et al., 1990). Small-footprint, discrete return Light Detection and Ranging (LiDAR), or airborne laser scanning, is not limited by many of these spectral challenges; however, separating LiDAR returns in low-height, open canopy rangeland vegetation is difficult because the vegetation canopy returns are often close to ground returns. Recent studies confirm the appropriateness of LiDAR for structural and biomass applications (Latifi et al., 2012; Swatantran et al., 2011; Zolkos et al., 2013), with hyperspectral data providing important canopy stress information (Swatantran et al., 2011) and minor improvements to the LiDAR models (e.g., Anderson et al., 2008; Latifi et al., 2012; Mundt et al., 2006). While combining LiDAR-derived estimates of vegetation structure with hyperspectral information tends to result in slightly improved accuracy, new methods are needed to optimize these datasets; understand the relative tradeoffs and redundancies between the two sensors; identify uncertainties associated with upscaling; and develop composite products that can be iteratively assessed and refined in terms of prediction accuracy (Esteban et al., 2005).

Furthermore, an improved understanding of the contribution of hyperspectral data in estimating vegetation structure will improve future applications of HyspIRI (Hyperspectral Infrared Imager) data, along with synergistic use of HypsIRI with other remote sensing data, such airborne hyperspectral and LiDAR, and ICESat-2's Advanced Topographic Laser Altimeter (ATLAS). HyspIRI is a future National Research Council (NRC) decadal survey mission from National Aeronautics and Space Administration (NASA) that is expected to be launched in the next decade (NRC, 2007). One of the instruments onboard HyspIRI is an imaging spectrometer yielding 60 m spatial resolution data in 10 nm contiguous bands ranging from 380 nm - 2500 nm at an equatorial 19 day repeat cycle (NASA, 2014). The spectral range and bandwidth is similar to that of the Hyperion sensor on NASA's EO-1 satellite. Hyperion can collect transect samples in narrow swaths at 30 m spatial resolution but suffers from cross-track calibration issues and is limited by low signal-to-noise (Pearlman et al., 2003). In contrast, HyspIRI is a global imager and the mission is primarily expected to contribute to our understanding of carbon and ecosystem processes by enabling global vegetation mapping at finer taxonomic levels and rapid detection of plant stresses. Recently, using simulated data, various studies have demonstrated the potential of HyspIRI in different applications such as vegetation mapping (Olsson & Morisette, 2014), estimation of fraction of photosynthetically active radiation and leaf water content (Zhang et al., 2012), and in other geoscience (Abrams et al., 2013; Kruse et al., 2011) and urban applications (Roberts et al., 2012). Similar studies on more complex shrubland ecosystems can provide insights into the potential of HyspIRI in estimating vegetation structural parameters such as cover and biomass. Airborne hyperspectral data obtained from NASA's AVIRIS sensor (limited availability due to commissioning requirement) or commercial instruments such as HyMap (HyVista Co., Sydney, Australia) contain similar spectral coverage and can be relevant proxies to generate such simulations.

This study analyzes and integrates HyMap and LiDAR data using a random forests approach (Breiman, 2001), which can be used to select (indirectly) important predictor variables and has been demonstrated to predict forest canopy structural measurements using LiDAR (Hudak et al., 2008) and spectral/LiDAR combinations (Guo et al., 2011; Leutner et al, 2012). Ensemble learning approaches such as random forests are well-suited to handle "wide-datasets" such as the datasets analyzed in this study because they result in smaller prediction variance and bias and better model performance compared to other approaches (e.g., Gislason et al., 2006; Mitchell et al., 2013; Pal, 2005; Rodriguez-Galiano, et al., 2012; Strobl et al., 2009).

In the first part of this study we explore the relative contributions of high resolution (3 m pixels) airborne HyMap and discrete return, small footprint LiDAR data to the estimation of shrub cover using ground reference data sampled across three collection sites that span precipitation and elevation gradients in the Great Basin region of southern Idaho, USA (Olsoy et al., 2014). We also consider uncertainty associated with combining all three sites for analysis. In the second part of this study, we simulate HyspIRI imaging spectrometer data to assess the potential for satellite hyperspectral data to estimate shrub cover and height at the regional scale (60 m pixels; across all three sites) using LiDAR-only metrics as a pseudo validation dataset. Findings are designed to provide insight into the extent to which hyperspectral satellite observations can augment structure measurements in dryland systems where future laser altimetry satellite technologies may be sensitive to areas of low canopy cover.

2. Methods

2.1 Study Sites

The study areas consist of three collection sites located across the sagebrush-steppe ecosystem in southern Idaho, USA (Figure 1): Department of Energy's Idaho National Lab (INL), Hollister, and Reynolds Creek Experimental Watershed (RCEW). The INL study site is located in cold desert sagebrush-steppe along the eastern Snake River plain in an intermountain landscape. The study area and its vicinity are flat, with elevations in the study area ranging from approximately 1479 to 1496 m. Microtopographical fluctuations created by historical agricultural practices, namely archaic irrigation channels and associated side channels, are present in the northeastern portion of the project area. The study site is dominated by Wyoming big sagebrush (*Artemisia tridentata* subsp. *wyomingensis*), while basin big sagebrush (*Artemisia tridentata* subsp. *tridentata*) occurs in association with depressional areas and drainage channels. Other species common to the study area include yellow rabbit brush (*Chrysothamnus viscidiflorus),* pricklypear cactus *(Opuntia spp.)* and crested wheatgrass *(Agropyron cristatum).*

The Hollister site is located in the County of Twin Falls in the Snake River plain region of southern Idaho. The study area is sloped southwest to northeast, with elevations ranging from approximately 1551 m in the southern portion to approximately 1362 m in the northern portion of the site. The plant community is Wyoming Big Sagebrush (*Artemesia tridentata ssp wyomingensis*) of low-stature (generally < 50 cm, all < 1 m) (Fig. 2a) and a relatively high ratio of wood: leaves. Herbaceous cover includes Sandberg's bluegrass and squirreltail (*Poa secunda* and *Elymus elemoides*, respectively) as dominant understory bunchgrasses and moderate and patchy occurrence of cheatgrass, crested wheatgrass, and native forbs. Fire history records indicate minimal disturbance.

The RCEW consists of approximately 239 km^2 of land located in the Owyhee Mountains in southwestern Idaho, USA. Elevations in the watershed range from 1049 to 2245 m. Sagebrush and grassland communities are the dominant vegetation cover (Fig. 2b). Common shrub species include low sagebrush (*Artemisia arbuscula* Nutt.), big sagebrush (*Artemisia tridentata* Nutt. subsp. *vaseyana* [Rydb.] Beetle and subsp. *wyomingensis*) and bitter brush (*Purshia tridentata* [Pursh] DC), which typically grow up to 50 cm, 50–100 cm, and 60–185 cm in height, respectively.

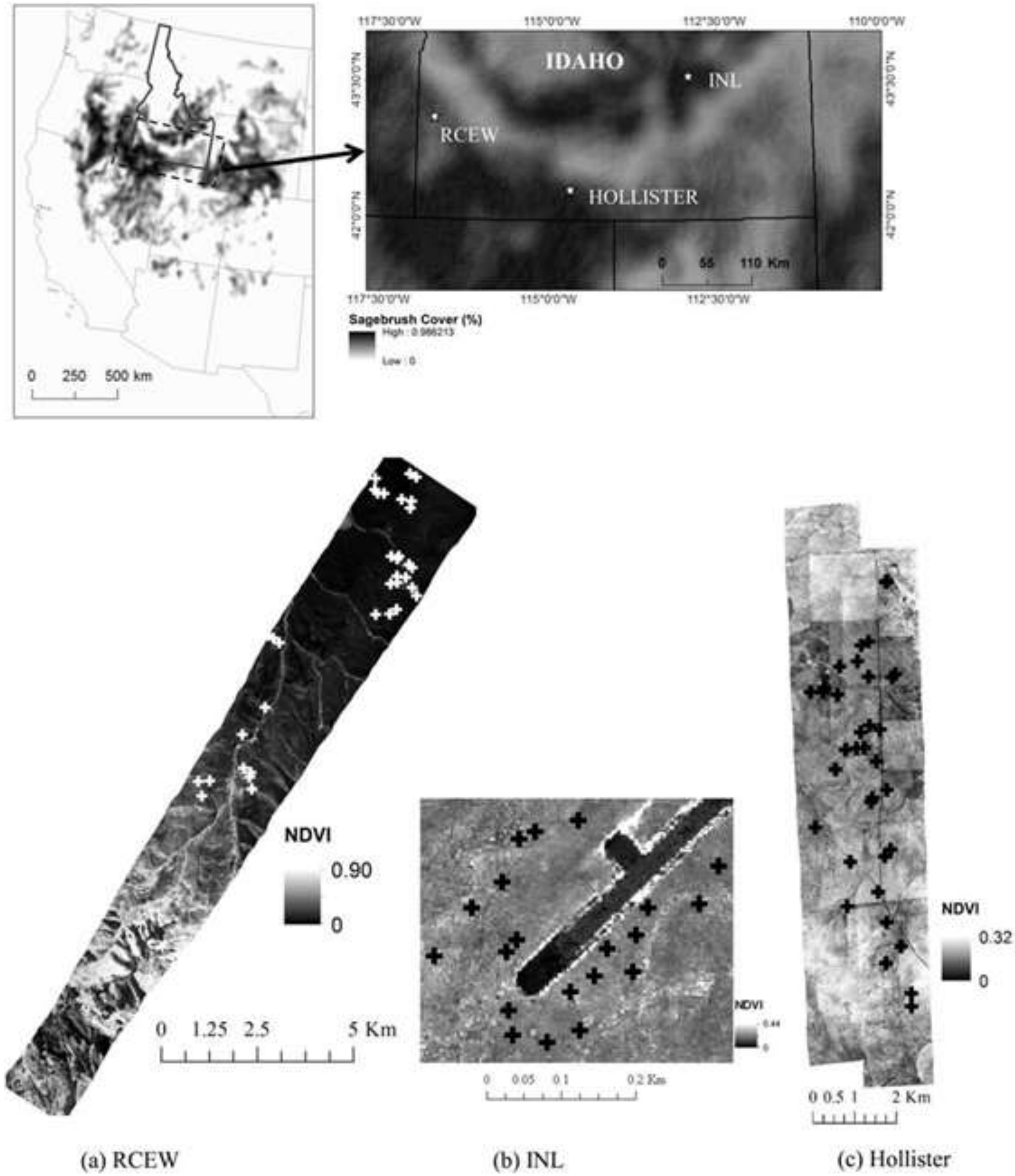

166

167 Figure 1. Locations of three collection sites in southern Idaho, USA: (a) RCEW, (b) INL, and (c)
168 Hollister. Shaded areas in the upper figure represent big sagebrush dominance across western US. Images
169 in lower figures are Normalized Differential Vegetation Index (NDVI). Field reference plots are depicted
170 as crosses.

(a) (b)

Figure 2. Photographs showing typical sagebrush (*Artemisia tridentata)* dominated areas at (a) Hollister and (b) RCEW study sites.

2.2 Data Collection

This cross-site shrub cover analysis was designed using ground reference and airborne HyMap and LiDAR data collected at three sagebrush-steppe sites in southern Idaho from 2007 to 2011 (Table 1). While individual site research was previously conducted at all three sites, new reference plots were established in the field in fall 2011 to support the analysis presented in this paper. All HyMap and LiDAR datasets were independent acquisitions. Data collection, both ground and airborne, were limited to late summer and early fall, when grass has senesced and sagebrush is still photosynthetically active, in order to minimize the influence of grass on shrub cover estimates.

Table 1: Field and remote sensing data collection in the three study sites: INL, Hollister, and RCEW.

Site	Field Sampling Plots	Hyperspectral (Hymap)	LiDAR
INL	Plots: *n* =20 (7 m X 7m) Date: 12 to14 Sept 2011	Pixel resolution: 3.1 m Date: 14 Aug 2010	Point Density: 10 pts m^{-2} Date: 05 Aug 2010
Hollister	Plots: *n* = 35 (10m X 10m) Date: 18 to 22 July 2011 & 02 to 03 August 2011	Pixel resolution: 2.1 m Date: 13 Aug 2010	Point Density: 10 pts m^{-2} Date: 05 Aug 2010
RCEW	Plots: *n* =23 (10m X 10m) Date: 14 to 15 July, 2011; 26 to 27 July 2011 & 01 to 09 August 2011	Pixel resolution: 3.0 m Date: 10 Aug 2010	Point Density: 6 pts m^{-2} Date: 11 to 18 Nov 2007

2.2.1 Field Data Collection

Field sampling plots (7 m X 7 m or 10 m X 10 m) were used to collect shrub cover, and in most cases, shrub height measurements at the INL, Hollister and RCEW sites from July to November 2011 (Table 1). For all sites, plot sampling locations were randomly generated. Once located, plot corners were marked and recorded using a positioning system with centimeter to submeter accuracy. Vegetation percent cover information was recorded along north-south transects spaced 1 m apart at each plot using a point intercept method (Greig-Smith, 1983). Presence, vegetation type, and ground type were recorded at 1 m intervals along each transect. The following categories were recorded: live (green and woody) and dead (decaying) components of sagebrush, rabbit brush, bitter brush, other shrubs, grass, herbaceous, litter, rock, and bare ground. For the study herein, we utilize the percent vegetation cover measurements for shrub only. Percent shrub cover was estimated for each plot by calculating the total number of points intercepted by live and dead shrubs (sagebrush, rabbit brush, bitter brush, and other shrubs), then dividing this total by the total number of point intercept measurements. Shrub height was recorded as the highest height at each point intercept sampling location (e.g. every 1 m), then averaged for each plot.

2.2.2 Hyperspectral Image Acquisition

HyMap imagery were collected over all three study sites (Fig. 1, Table 1) using the HyMap sensor (operated by HyVista, Inc.), which collects calibrated data in 126 near-contiguous spectral bands (450–2480 nm) that range in width from 15 nm in the visible and near infrared to 20 nm in the shortwave infrared (Cocks et al., 1989).

2.2.3 LiDAR Data Acquisitions

LiDAR data were acquired for all three study sites using a dual-mounted Leica ALS50 Phase II sensor mounted in a Cessna Caravan 208B operated by Watershed Sciences Inc., Corvallis, Oregon, USA (Table 1). The sensor operates at a wavelength pulse of 1064 nm and has a vertical discrimination height of 2.8 m, which resulted in only the first return from each pulse being recorded in our study plots. The data were acquired at a pulse rate of 83 kHz and with a 28° field of view during the 2007 and 2010 flights, and with an estimated pulse beam diameter of 0.20 m on the ground (at nadir) during the 2007 flights. Absolute vertical accuracy of the INL and Hollister datasets were assessed by the vendor using RTK GPS of ground control points (n = 912) and was estimated to have a root mean square error (RMSE) of 0.03 m. Vertical accuracy of the dataset was assessed using ground elevation points (n = 52) collected with a RTK GPS over a flat gravel parking lot. The closest LiDAR point to each GPS location was determined and the elevations were compared to calculate RMSE, which resulted in an estimated vertical accuracy of 0.10 m (Glenn et al., 2011).

2.3 Hyperspectral and LiDAR Processing

All data processing, unless otherwise stated, was performed using the Environment for Visualizing Images (Boulder, Colorado, USA). Radiometric and geometric corrections were applied to the HyMap imagery using files provided by the vendor. Radiance values were converted to apparent reflectance using the HyCorr2 (HyMap Correction) absolute atmospheric correction modeling package, which was developed by the CSIRO (Commonwealth Scientific and Industrial Research Organization), Australia and is based on the Atmospheric Removal Program (ATREM; Gao & Goetz 1990; Gao et al., 1992). The absolute atmospheric corrections produced scaled surface reflectance values that account for scattering and absorption of solar radiation by the earth's atmosphere. Such corrections are relevant to this study because they enable data recorded at the sensor to be directly compared to data recorded on the ground and to other remotely sensed images obtained under different atmospheric conditions (i.e., comparisons among HyMap images collected on different dates at multiple study sites). Surface reflectance measurements were collected for calibration tarps with 2.5%, 24%, and 56% reflectivity (Group VIII Technologies, Inc., Provo, UT, USA) at the time of overflights at the INL site using a FieldSpec Pro spectroradiometer (PANalytical, Boulder, CO, USA). These *in situ* surface reflectance values were compared to the atmospherically corrected reflectance values of corresponding pixels in the imagery. Comparisons indicated consistency in brightness across wavelengths but the data were not used to radiometrically correct the imagery. After converting images to surface reflectance in HyCorr2, illumination error remained visually apparent in the cross-track direction for all individual flightlines and was attributed to differences in viewing geometries and forward and backward scattering in areas of flightline overlap. Before mosaicking flightlines for each study area, a standard multiplicative cross-track correction offered in ENVI was applied to each flightline using a first polynomial fit for each band. The corrections effectively flattened reflectance data and compensated for brightness in the far western columns of the images.

LiDAR data were height filtered and processed into raster topographic and vegetation products in using the BCAL LiDAR Tools developed for semiarid vegetation (http://bcal.boisestate.edu/tools/lidar; Streutker & Glenn 2006). LiDAR data were height filtered using a 5 m canopy spacing, a 5 cm ground threshold, nearest neighbor interpolation, and 30 iterations to separate ground and vegetation returns. LiDAR-based raster surfaces were generated at the 3 m pixel resolution (to match HyMap data) using the point cloud data across 3 m areas and included metrics such as percentage of ground returns, height interquartile range, canopy relief ratio, total point density, vegetation roughness, and local roughness (Table 2).

Table 2. LiDAR variables used in analysis (calculations described are per pixel).

LiDAR	**Description**
H_{range}	Difference between maximum and minimum height of all vegetation returns
H_{mean}	Average height of all LiDAR vegetation returns
H_{MAD}	Median Absolute Deviation (MAD) from median height of all LiDAR vegetation returns; MAD = 1.4826 x median(|height - median height|)
H_{AAD}	Mean Absolute Deviation (AAD) from mean height of all LiDAR vegetation returns; AAD = mean(|height - mean height|)
H_{var}	Variance of height of all LiDAR vegetation returns
H_{stdev}	Standard deviation of height of all LiDAR ground returns
H_{skew}	Skewness of height of all LiDAR vegetation returns
H_{kurt}	Kurtosis of height of all LiDAR vegetation returns
H_{IQR}	Interquartile Range (IQR) of height of all LiDAR vegetation returns; IQR = Q75-Q25, where Qx is x^{th} percentile
H_{CV}	Coefficient of variation of all LiDAR vegetation returns
H_{nthP}	The 5th, 10th, 25th, 50th (median), 75th, 90^{th,} and 95th percentiles of all LiDAR vegetation returns
H_{CNR}	Canopy relief ratio (CNR) of height (H) of LiDAR vegetation returns CNR = $((H_{mean} – H_{min}))/((H_{max} – H_{min}))$
H_{text}	Texture of height of LiDAR vegetation returns; Texture = St. Dev. (Height > Ground Threshold and Height < Crown Threshold)
Veg_Cov	Percent ratio of LiDAR vegetation returns (greater than 0.15m height) and total returns
Veg_Density	Percent ratio of LiDAR vegetation returns and ground returns
$N_{per\_g\_ret}$	Percent ratio of LiDAR ground returns (≥ 0.15m height) and total returns
N_{return}	Total number of all LiDAR returns
N_{v_return}	Total number of all LiDAR returns greater than 0.15m height
N_{g_return}	Total number of all LiDAR returns less than 0.15m height

HyMap mosaics were poorly rectified and consequently co-registered to 3 m LiDAR raster data by specifying 10 coincident ground control points at each study site to warp the HyMap bands. In all cases a nearest neighbor 1st degree polynomial resampling method was applied to the imagery, which resulted in RMSE values less than 1 pixel (3 m) for the co-registered datasets. Ground control points were selected in the rasters using a combination of true color and color infrared displays of the HyMap imagery and intensity and maximum vegetation height displays of the LiDAR raster products.

Co-registered HyMap and LiDAR datasets were processed for the purpose of identifying variables relevant to estimating shrub cover. A majority of vegetation indices are calculated as ratios or normalized ratios of two or more bands used to calculate a single index that is sensitive to a biophysical or biochemical variable of interest. The mosaics were processed by calculating a series of vegetation indices related to greenness (broadband and narrowband), light use efficiency, senescent vegetation, and canopy water content (Table 3). These vegetation indices were considered given the potential for correlations between shrub cover and spectral calculations that enhance plant processes and biochemical content, as shown by various studies (e.g. Purevdorj et al., 1998). The LiDAR approach to estimating percent shrub cover was to sum the number of vegetation returns greater than 15 cm and divide by the total number of returns. The 15 cm threshold is considered an optimal height for accounting for 1) relative and absolute vertical accuracy of the LiDAR system, 2) error associated with confusion between ground and vegetation returns in sagebrush steppe environments, and 3) noise associated with microtopographical relief (Mitchell et al., 2011; Smith et al., 2009; Spaete et al., 2011; Streutker et al., 2011). An examination of the distribution of LiDAR vegetation returns by canopy height across ground reference plots at the point cloud scale is consistent with the 15 cm threshold for calculating shrub cover (Fig. 3).

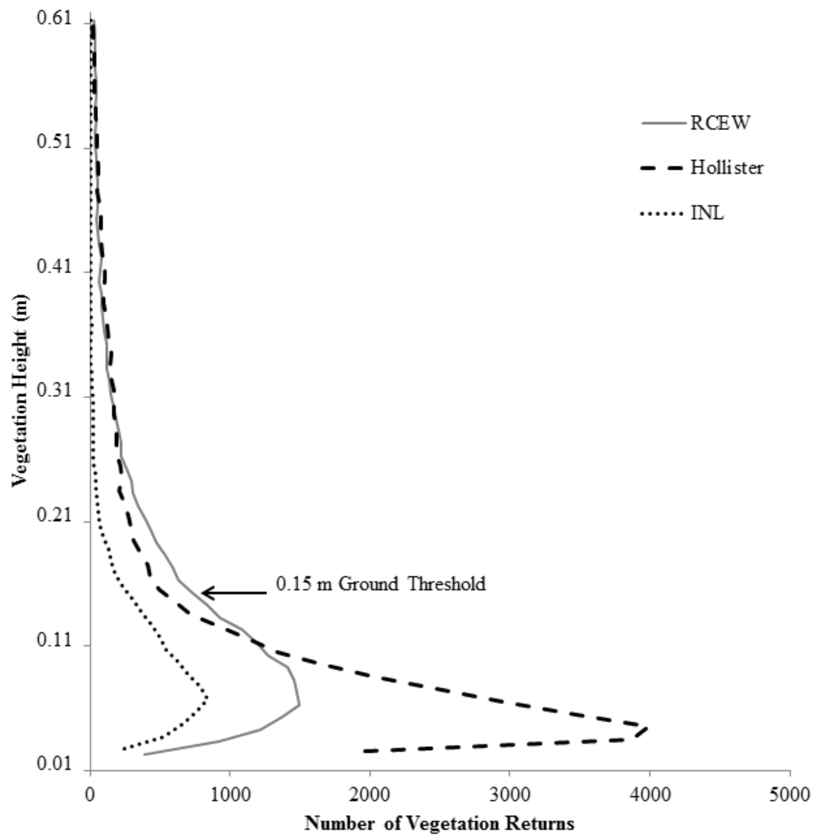

Figure 3: Distribution of LiDAR vegetation returns, binned by height, and spatially subset to the field reference plots at RCEW (n = 23), Hollister (n = 35), and INL (n =20) study sites.

Table 3. Vegetation indices used in analysis.

Index	**Formulation** (R = reflectance, wavelengths in nm)	**Reference**
Normalized Difference Vegetation Index	$NDVI = (R_{NIR} - R_{Red}) / (R_{NIR} + R_{Red})$	Rouse et al., (1973)
Green Normalized Difference Vegetation Index	$GNDVI = (R_{NIR} - R_{GREEN}) / (R_{NIR} + R_{GREEN})$	Gitelson & Merzylak (1996)
Red Edge Normalized Vegetation Index	$NDVI_{705} = (R_{750} - R_{705}) / (R_{750} + R_{705})$	Gitelson & Merzlyak (1994)
Simple Ratio Index	$SRI = R_{NIR} / R_{RED}$	Tucker (1979)
Enhanced Vegetation Index	$EVI = 2.5(R_{NIR} - R_{RED})/(R_{NIR}{}^{6} R_{RED}{}^{-1.5} R_{BLUE})$	Huete et al. (1997)
Red Edge Position Index	REPI = Maximum value* from 690 to 740 nm region	Curran et al. (1995)
Normalized Difference Lignin Index	$NDLI = (\log R_{1510} - \log R_{1680}) / (\log R_{1510} + \log R_{1680})$	Serrano et al. (2002)
The Plant Senescence Reflectance Index	$PSRI = (R_{680} - R_{500}) / R_{750}$	Merzlyak et al. (1999)
Water Band Index	$WBI = R_{900} / R_{970}$	Penuelas et al. (1997)
Normalized Difference Infrared Index	$NDII = (R_{819} - R_{1649}) / (R_{819} + B_{1649})$	Hardisky et al. (1983)
Moisture Stress Index	$MSI = R_{1599} / R_{819}$	Hunt & Rock (1989); Ceccato et al. (2001)
Vogelmann Red Edge Index 1	$VOG1 = R_{740} / R_{720}$	Voggelman et al. (1993)
Vogelmann Red Edge Index 2	$VOG2 = (R_{734} - R_{747}) / (R_{715} - R_{726})$	Voggelman et al. (1993)
Vogelmann Red Edge Index 3	$VOG3 = (R_{734} - R_{747}) / (R_{715} - R_{720})$	Voggelman et al. (1993)
Red Green Ratio	$RG\ Ratio = R_{RED} / R_{GREEN}$	Gamon & Surfus (1999)
Photochemical Reflectance Index	$PRI = (R_{531} - R_{570}) / (R_{531} + R_{570})$	Gamon et al. (1997)
Sum Green Index	SGI = Normalized mean reflectance from 500 to 600 nm	Lobell & Asner (2003)
Carotenoid Reflectance Index 1	$CRI1 = (1/R_{510}) - (1/R_{550})$	Gitelson et al. (2002)
Carotenoid Reflectance Index 2	$CRI2 = (1/R_{510)}) - (1/R_{700})$	Gitelson et al. (2002)
Anthocyanin Reflectance Index 1	$ARI1 = (1/R_{550}) - (1/R_{700})]$	Gitelson et al. (2001)
Anthocyanin Reflectance Index 2	$ARI2 = (800*(1/R_{510}) - (1/R_{700})$	Gitelson et al. (2001)

*Derivative reflectance (Dixit & Ram, 1985).

2.4 Shrub Cover Estimation at 3m Spatial Resolution

Random forests (Brieman, 2001) and the accompanying Gini Index criteria were used to evaluate the extent to which hyperspectral and LiDAR variables (Table 4) could predict shrub cover at pixel locations unsampled in the field. All three sites were analyzed collectively and the most important shrub cover predictor variables were identified (Salford Predictive Modeler Software Suite version 7, Salford Systems, San Diego, CA). The random forests method is nonparametric and based on an iterative machine learning algorithm that uses an ensemble of randomly generated regression trees. Random forests addresses limitations associated with overfitting and instability that can arise when using conventional regression tree-based approaches. Multiple bootstrap samples from the original training dataset and predictor variables are selected (with replacement) to generate a large number of non-linear trees; predictions for each tree are used in a voting process. Final prediction success is computed by averaging prediction success across each tree in the forest (Pal, 2005). The selection of variables at each node of the tree is based on a measurement of variable importance called the Gini index (Breiman et al., 1984). The Gini index represents a degree of node impurity, computed as the difference between out-of-bag error and the error from a permutated subset of data at each node. The random forests method includes a built-in robust validation that uses random subsets of both the data and the predictors bootstrapped several hundreds of times. The fit of random forests regression model are evaluated by r^2 and the RMSE values from out-of-bag testing. The coefficient r^2 is sometimes also referred by the term "pseudo R-squared" and is the percent variance explained computed as 1 - (mean square error)/(variance (target response)).

Once a final random forests model is selected after iterative runs to remove the least important variables, a nearest neighbor imputation method is typically used to generate a spatially explicit raster surface (Crookston & Finley, 2008). This estimated response surface contains predicted values for the variable of interest (e.g., shrub cover) at unsampled locations. Usually, imputation implies estimating the variable of interest from a set of *k* nearest neighbors within the dataset. When $k = 1$, the imputed value is assigned from the nearest neighbor, and when $k > 1$, other methods employing either a weighted distance or a random forests proximity matrix are used for finding nearest neighbors (Crookston & Finley, 2008). Instead of Euclidean distance, random forests imputation uses statistical distance, which can be computed using a proximity matrix or nonparametric methods.

At the 3 m spatial resolution, HyMap and LiDAR predictor variables identified in Table 4 were used to run the initial random forests model. A total of 2000 trees were generated for each run. The maximum number of variables considered per node was held equal to the square root of the number of variables for the run, as suggested by Breiman (2001). After the first run, the least important variable was removed and a new random forests model was built with the remaining variables. This process was repeated until error between iterations remained constant. The final model consisted of the smallest set of variables with the minimum out-of-bag error rate. This "back-ward elimination" approach to selecting variables is widely used in the literature (e.g. Dıaz-Uriarte & Alvarez de Andres, 2006; Falkowski et al., 2010; Hudak et al., 2008) and found to preserve important variables and eliminate redundant variables (Vauhkonen, 2010). The variables selected in random forests were used to generate a final wall-to-wall shrub cover predicted response surface for all three sites by implementing the R package yaImpute (Crookston et al., 2008; http://cran.us.r-project.org/; version R 2.12.2), which has a built-in random forests distance matrix (Hudak et al., 2008).

Table 4. Variables used in random forests analysis.

Spectral variables	LiDAR variables
HyMap Reflectance bands (*n* =125)	H_{range}
HyspIRI reflectance bands (*n* =211)	H_{mean}
NDVI	H_{MAD}
Simple Ratio Index (SRI)	H_{AAD}
Enhanved Vegetation Index (EVI)	H_{var}
Red Edge NDVI	H_{stdev}
Red Edge Position (REP)	H_{skew}
Normalized Difference Lignin Index (NDLI)	H_{kurt}
Plant Senscence Reflectance Index (PSRI)	H_{IQR}
Water Band Index (WBI)	H_{CV}
Moisture Stress Index (MSI)	H_{nthP}
Normalized Difference Infrared Index (NDII)	H_{CNR}
GNDVI	H_{text}
NDVI705	Veg_Cov
Sum Green Index	Veg_Density
Red: Green (R:G)	$N_{per\_g\_ret}$
Photochemical Reflectance Index (PRI)	N_{return}^{*}
Vogelmann Index 1 (VOG1)	$N_{v\_return}^{*}$
Vogelmann Index 2 (VOG2)	$N_{g\_return}^{*}$
Carotenoid Reflectance Index 1 (CAR1)	
Carotenoid Reflectance Index 2 (CAR2)	
Anthocyanin Reflectance Index 1 (ARI1)	
Anthocyanin Reflectance Index 2 (ARI2)	

* While these variables do not have a physical basis for inclusion in the random forests analysis, they were retained but not selected for analysis nor used in subsequent mapping.

2.5 HyspIRI-simulated Estimation of Shrub Cover and Height at 60 m Spatial Resolution

At the 60 m spatial resolution, we performed a HyspIRI simulation to test the extent to which hyperspectral satellite observations could estimate shrub cover and vertical structure measurements (i.e., shrub height) across dryland landscapes. To simulate HyspIRI observations, HyMap imagery (472 – 2487 nm; ~ 13 – 206 nm full width half maximum (FWHM); 125 bands) were spectrally resampled to match higher spectral resolution HyspIRI channels (470 – 2477 nm; ~ 9 - 12 nm FWHM; 211 bands) using Gaussian models defined by instrument FWHM values. A comparison of the average reflectance spectra between Hymap and HyspIRI-simulated imagery is shown in Fig. 4. After spectral resampling, the HyspIRI imagery were spatially averaged from a 3 m pixel resolution to a 60 m pixel resolution. To evaluate the simulations, we related HyspIRI-simulated reflectance bands and vegetation indices on a pixel basis to four different LiDAR variables averaged from 3 m pixel resolution to 60 m pixel resolution: (1) ratio of vegetation returns to total returns (hereafter referred to as "LiDAR ratio of returns"), (2) LiDAR-only shrub cover derived from random forests estimates in Section 2.4, (3) mean vegetation height, and (4) maximum vegetation height.

LiDAR ratio of returns has been used as a surrogate for true vegetation cover in forested ecosystems (e.g. Smith et al., 2009); however, in ecosystems dominated with low-stature shrubs, where only a few LiDAR returns are reflected from vegetation, this ratio may not be a robust metric for estimating vegetation cover. Therefore, we also considered the shrub cover derived from LiDAR-only variables in random forests. Using the combined LiDAR and HyMap shrub cover product would have biased our results because the surrogate validation dataset and the HyspIRI-simulated dataset contain the same spectral information. Height measurements collected in the field for this study did not support validation of LiDAR height variables. Consequently, LiDAR mean and maximum vegetation height variables were used as surrogate validation datasets. A series of related studies on sagebrush height estimation using discrete return airborne LiDAR found moderate to strong agreement between these variables (r^2 from 0.58 to 0.86) and the height of individual shrubs measured in the field (Streutker & Glenn, 2006, Mitchell et al., 2011). These sagebrush height studies consistently noted height underestimation on the order of 30 cm or approximately 30% of an average shrub, with limited error introduced by slopes less than 15% (Glenn et al., 2011, Spaete et al., 2011).

To perform the analysis, a sample of 200 training locations (60 m pixels) was randomly selected in each study area from the simulated HyspIRI imagery. For each selected 60 m pixel, reflectance values and a series of vegetation indices were related to LiDAR-derived shrub cover and height estimates. A total of 232 predictor variables were used for the initial random forests run: individual HyspIRI-simulated bands (*n* = 211) and vegetation indices (*n* =21). The random forests approach was similar to that described in section 2.5. The model accuracies in terms of out-of-bag estimates of r^2 and RMSE are reported. In addition, a separate set of test data consisting of 100 samples from each of the three study areas were randomly selected and used to test the strength of the model. The random forests model with the best subset of variables was then used to create a wall-to-wall predicted surface of shrub cover map at 60 m resolution.

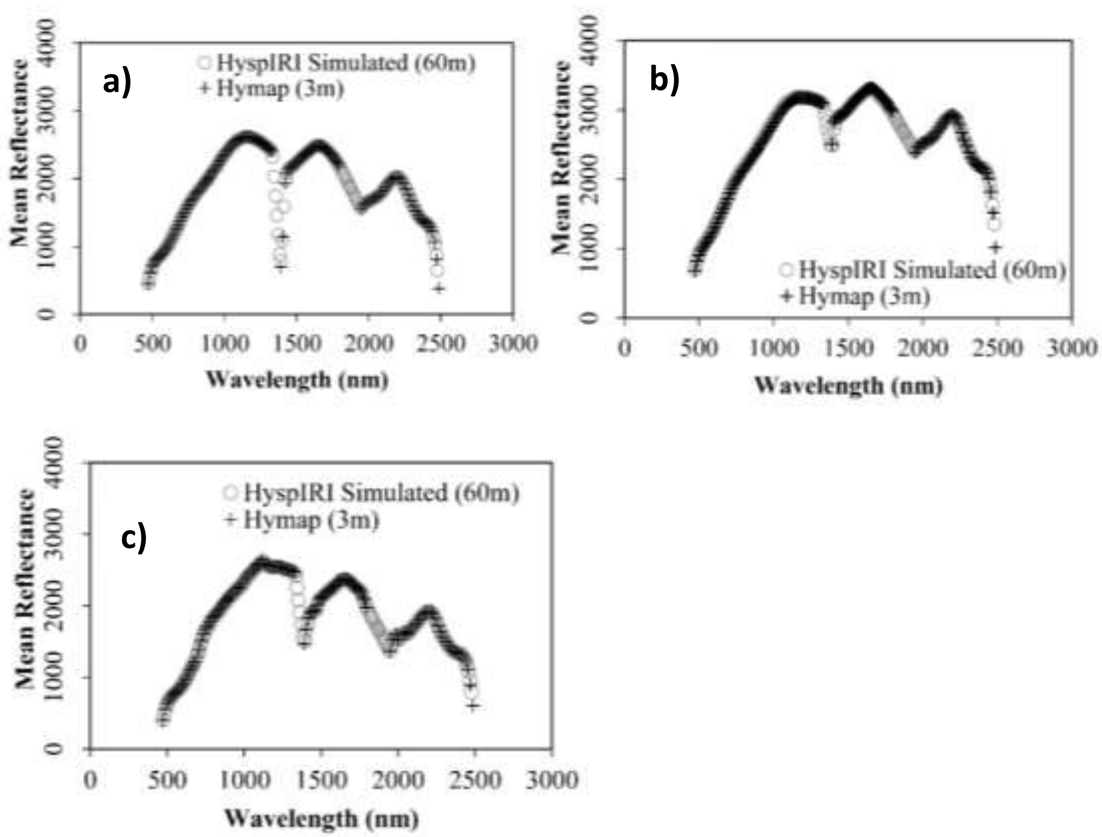

Figure 4: The average reflectance spectra of HyspIRI-simulated (60 m) and Hymap (3 m) grids at the three study sites: (a) INL (b) Hollister and (c) RCEW.

3. Results and Discussion

3.1. Field Data

Shrub cover among all the sites ranged up to 45%, except for the INL site which had one plot with 52% shrub cover (Table 5). However, there were 9 sample plots with less than 10% cover at INL, compared to only 1 and 3 plots at RCEW and Hollister respectively. The RCEW plots had the highest median shrub cover (31%), followed by Hollister (21%) and INL (17%). Average shrub vegetation heights ranged from 8 to 71 cm across the sites.

Table 5. Summary of shrub cover and height measurements collected at the three study sites in Hollister, INL and RCEW.

	Hollister (*n* = 35)			**INL (*n* = 20)**			**RCEW (*n* = 23)**		
	Median ± SE†	**Min**	**Max**	**Mean ± SE**	**Min**	**Max**	**Mean ± SE**	**Min**	**Max**
Shrub cover (%)	21.5± 1.5	1.7	41.3	17.2± 3.3	0.0	51.6	30.6± 2.0	9.9	44.6
Shrub height (cm)	42.1± 1.7	25.1	59.6	50.4± 3.9	8.2	70.8	24.0± 5.8‡	20.0	63.1

†SE = Standard error of mean; ‡Vegetation heights were only recorded for 8 sample plots

3.2 Shrub Cover Estimation at 3 m Spatial Resolution

At the 3 m spatial resolution, the random forests model with both LiDAR variables and HyMap variables combined performed better than the model run with only LiDAR variables (r^2 of 0.58 and 0.49, respectively; Table 6). A total of 5 to 6 predictor variables were selected in the final random forests models for shrub cover based on minimum error and model parsimony. Among the LiDAR variables, median absolute deviation from the mean height (H_{MAD}), interquartile range of height of all vegetation returns (H_{IQR}), vegetation cover (Veg_Cov), texture of the height of the vegetation returns (H_{text}), vegetation density (Veg_Density), and the 5th percentile of vegetation returns (H_{5thP}) were ranked as the most important variables. When the HyMap and LiDAR data were combined, the HyMap variables of importance included the Anthocyanin Reflectance Index 2 (ARI2) and the red to green ratio; and the LiDAR variables included H_{IQR}, H_{MAD}, and Veg_Cov.

Shrub cover maps (Fig. 5 a-c) , which were generated from the LiDAR-only random forests model (Table 6), and used as a surrogate validation dataset for HyspIRI-simulated shrub cover (Table 7), had a strong tendency to overestimate field-measured shrub cover and by as much as 27.6% (but generally within 10.4%) for all three sites combined (Fig. 5 d). Overestimation results are likely due our inability to completely isolate shrub cover estimates from the influence of grass. The use of a single height threshold (0.15 m) for calculating Veg_Cov and Veg_Density variables with the point cloud data (Table 6) minimizes, but does not eliminate all grasses. The extent to which the threshold minimizes grass influence can vary across sites. For example, the threshold is less effective at RCEW, where taller grasses occurred more frequently (Fig. 3). Also, other LiDAR variables calculated from the point cloud data, such as $H_{MAD,}$ $H_{IQR,}$ and H_{5thP}, did not use the 0.15 m threshold and are even more likely to include grasses. Finally, the LiDAR calculations were performed using returns within a 3 m x 3 m area rather than within the actual ground reference plot boundaries, which can also influence cover estimation results.

Table 6. Results of shrub cover analysis with random forests using LiDAR only and both LiDAR and HyMap variables.

Source of predictor variables	**Predictor variables selected**[†]	r^2	**RMSE**
LiDAR-only	H_{MAD} H_{IQR} Veg_Cov H_{text} Veg_Density H_{5thP}	0.49	8.19%
HyMap + LiDAR	H_{IQR} H_{MAD} ARI2 Veg_Cov R:G	0.58	7.35%

[†] The order of the variables, ranking from most important top to bottom, indicates the variable importance as selected using Gini Index in random forests.

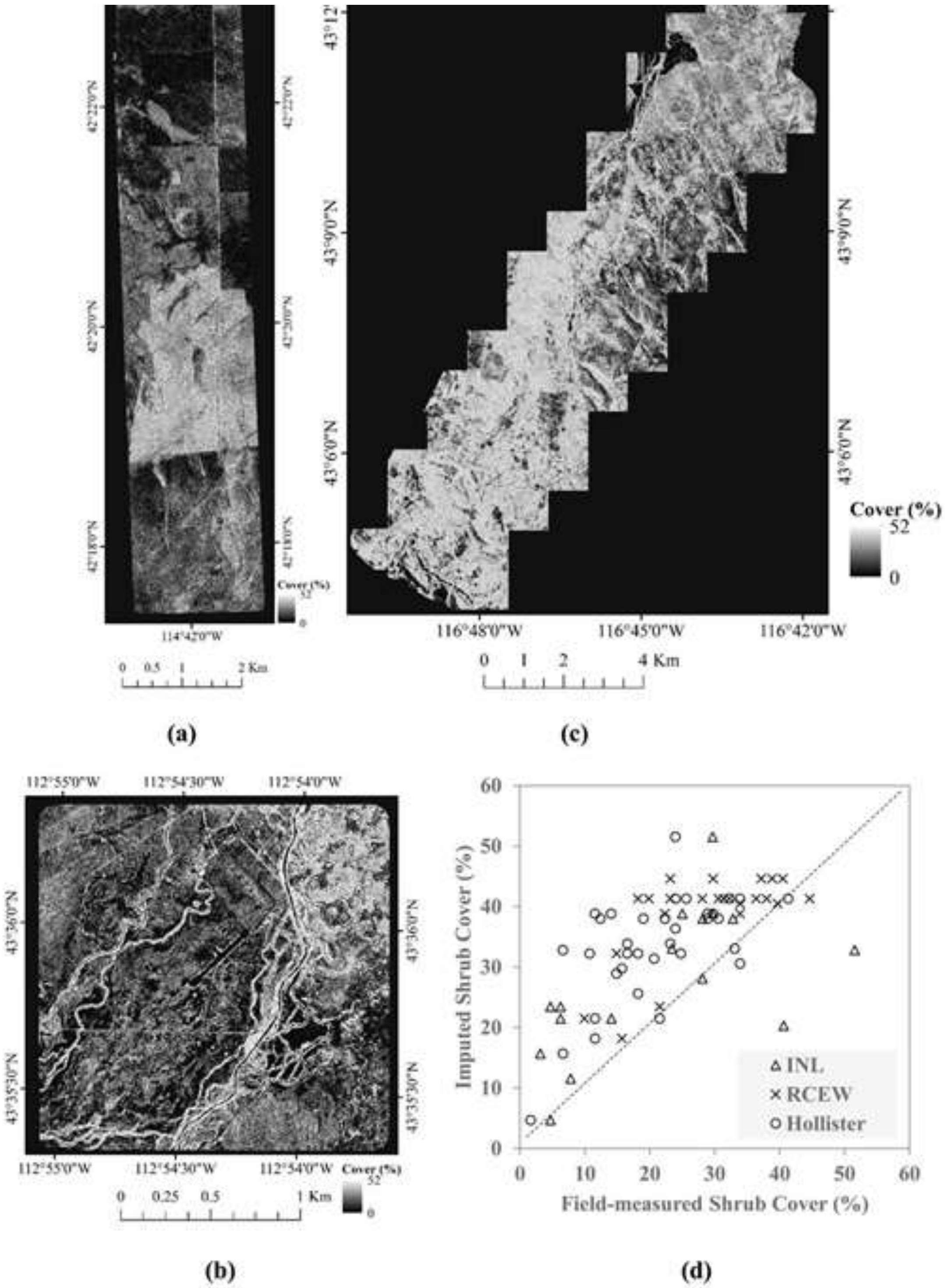

Figure 5. Imputed shrub cover (3 m resolution) using LiDAR metrics at the three study sites: (a) Hollister (b) RCEW and (c) INL. The actual vs imputed shrub cover relationship is shown in (d).

3.3 HyspIRI –simulated Estimation of Shrub Cover and Height at 60 m Spatial Resolution

HyspIRI-simulated variables estimated shrub cover and height (using the LiDAR-derived surrogate validation sets) resulted in r^2 values that ranged from 0.63 to 0.71 (Table 7; Fig. 6). For shrub cover, HyspIRI estimates were slightly more related to the cover version derived from LiDAR variables using random forests ("imputed") than to the LiDAR ratio of returns version, with the former producing almost half the error compared to the latter (RMSE of 4.94% and 8.72% respectively; Table 7). As expected for low stature vegetation, where there are only a few LiDAR returns reflected from the top of the canopy, the mean LiDAR height had lower error and higher correlation coefficient compared to the maximum LiDAR height (Table 7).

Among HyspIRI-simulated variables used to estimate shrub cover and height, the water band index (WBI; Table 3) was among the top five most important variables for both shrub cover estimated from LiDAR variables using random forests and shrub cover estimated using the LiDAR ratio of returns (Table 7). The WBI is associated with a strong water absorption feature around 900 nm and has been found to correlate well with greenness in semiarid shrubland ecosystems (Claudio et al., 2006). The red edge normalized difference vegetation (RENDVI or $NDVI_{705}$; Table 3) was the variable most relatable to shrub cover as calculated from the LiDAR ratio of returns. The index was designed for hyperspectral sensors and is sensitive to small changes in the vegetation red edge and therefore canopy foliage and senescence (Geitelson & Merzlyak, 1994; Sims & Gamon, 2002). The Vogelmann red edge indices (VOG1 and VOG2; Table 3) from the HyspIRI simulation were strong predictors of shrub cover estimated from LiDAR variables using random forests and of mean and maximum LiDAR shrub heights. These indices are also narrowband reflectance measurements and sensitive to chlorophyll content, leaf area, and water content (Vogelmann, 1993). Overall, HyspIRI-simulated variables of greatest importance were related to the red edge, water content and anthocyanins. A visual comparison of shrub cover maps derived from LiDAR variables using random forests to shrub cover maps derived from HyspIRI variables using random forests indicate general agreement, with some differences in distribution patterns likely attributable to resolution. The LiDAR cover version was originally estimated at 3 m and then averaged to 60 m while the HyspIRI cover was estimated directly at 60 m (Fig. 7). There was a somewhat jagged artifact to the LiDAR-derived shrub cover distributions; the range of the HyspIRI-simulated shrub cover values was smaller than that of the LiDAR-derived shrub cover; and there were noticeably greater peaks in the central tendencies of the shrub cover maps derived from HyspIRI-simulated variables. These differences were consistent across all three sites (Fig. 7).

Table 7. Results of using HyspIRI-simulated variables (*n*=200 samples in each of the three study areas and 232 bands) to estimate shrub cover and height (using LiDAR-derived variables as surrogate validation datasets). Analysis was performed using random forests and LiDAR variables were spatially coarsened from 3 m to 60 m pixels.

Predicted Variable	**Predictors**†	$r^{2‡}$	**RMSE**
LiDAR ratio of returns (vegetation returns : total returns)	RENDVI (100) REPI (74.58) WBI (58.38) MSI (32.94)	0.63	8.72%
LiDAR-only shrub cover from random forests	WBI (100) VOG2 (40.03) PSRI (39.96) NDLI (36.95) NDII (18.65)	0.65	4.94%
LiDAR vegetation height (mean)	VOG1 (100) ARI2 (19.75) RENDVI (15.60) REPI (12.05)	0.71	0.12 cm
LiDAR vegetation height (max)	VOG2 (100) VOG1 (58.74) ARI2 (22.69)	0.66	0.40 cm

† The order of the variables indicates the variable importance as selected using Gini Index in random forests. The variables at the top of the list are more important than those down the order. Gini index scores are indicated in parentheses.

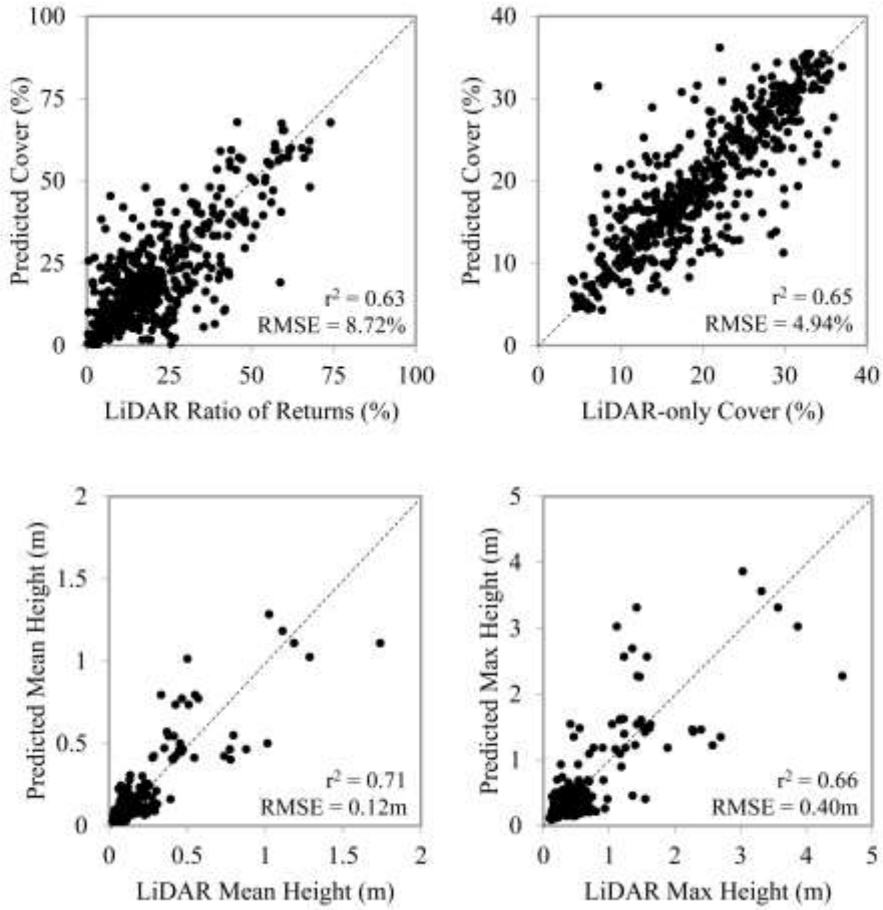

Figure 6. Actual vs predicted plots (*n*=600) from random forests regression of LiDAR-based shrub cover and height (aggregated to spatial resolution of 60m) with HyspIRI-simulated variables using *n*=200 samples in each of the three study areas and 232 bands.

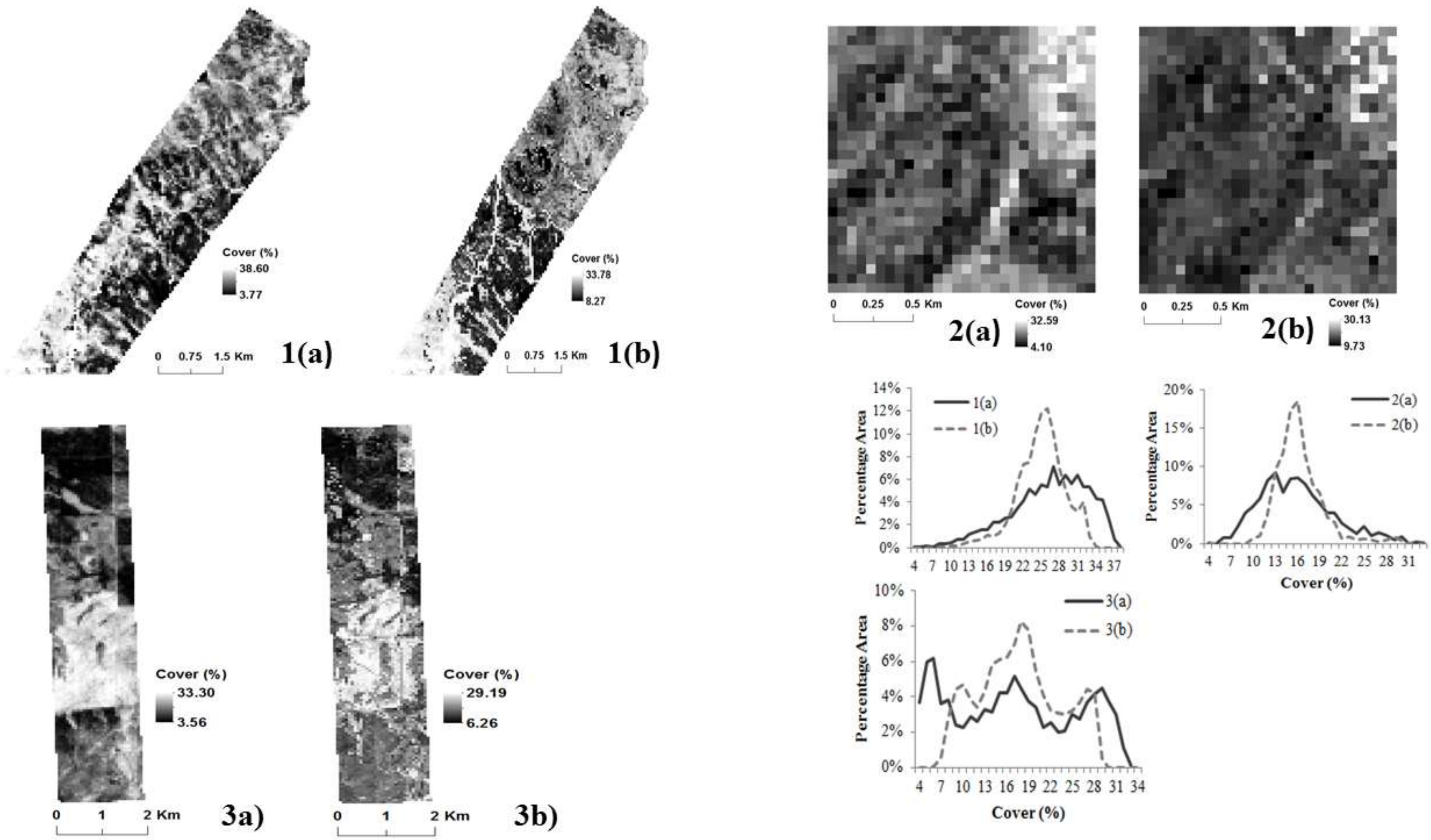

Figure 7. Imputed shrub cover at 60 m resolution in (1) RCEW, (2) INL, and (3) Hollister study areas. Shrub cover imputed using LiDAR only variables (using the random forests model in Table 6) (a) is compared to shrub cover imputed using HyspIRI-simulated bands (using the random forests model in Table 7) (b). Graphs show shrub cover distribution under scenarios (a) and (b) in the three study sites.

4. Discussion and Conclusions

A number of study limitations should be brought to the readers' attention before discussing the relative contributions of HyMap and LiDAR variables to predicting shrub cover at high resolution and the projected ability of HyspIRI to estimate shrub cover and height in dryland systems. One limitation is the time lag between field collection dates and HyMap and LiDAR acquisitions (see Table 1). In semi-arid environments, where shrubs grow slower due to low leaf area index and photosynthesis levels (Zeng et al., 2008), a one year gap between field and remote sensing collections may not have affected the structure and composition of the vegetation significantly. However, the four-year gap between LiDAR acquisition and field data collection at the RCEW collection site may have affected some structural metrics, such as cover. Between 2007 and 2011, the RCEW site received higher precipitation in the later years near the time field data collection occurred, which would have accelerated plant growth and exacerbated differences in cover measurement (precipitation: 235.1 mm (2007), 232.5 mm (2008), 323.5 mm (2009), 375.3 mm (2010), and 300.8 (2011) (USDA ARS, 2014). Another limitation is error introduced because of inherent discrepancies between field measurements and higher-precision LiDAR sampling and confusion between shrub and grass. In addition, we used a Gaussian model rather than spline interpolation to spectrally resample from low resolution HyMap data to higher resolution HyspIRI-simulated data. Another consideration is cross-track illumination error associated with HyMap flightline mosaics – a factor that would theoretically have less of an influence of HyspIRI swaths. Finally, at the HyspIRI-simulated 60 m spatial resolution, we used airborne LiDAR-derived cover estimates as a surrogate validation dataset despite recognized limitations associated with LiDAR discrimination of short-stature vegetation. Because only one source of hyperspectral data was available, the imagery could not be used for both validation (at

3 m) and testing (at 60 m).

At fine scales, this study demonstrates the potential for employing a single model consisting of canopy metrics and vegetation cover from LiDAR, complemented with airborne hyperspectral vegetation indices, to accurately estimate shrub cover. Our approach to couple LiDAR and spectral measurements is based on previous work (Leutner et al., 2012; Mundt et al., 2006) and demonstrates that shrub cover can be predicted using a random forests approach that includes the identification of important predictor variables. Among the selected important LiDAR variables, H_{MAD}, H_{IQR} and Veg_Cov (Table 2) were ranked higher in both the LiDAR-only and the HyMap / LiDAR combined models. H_{MAD} is a robust metric that captures the variability of height. Similarly, H_{IQR} captures the variability in the mid-region of the shrub where the bulk of LiDAR points are usually distributed. Another result to note is that Veg_Cov was ranked lower in importance than both H_{MAD} and H_{IQR} variables (Table 6). While Veg_Cov has been used as a surrogate for vegetation cover in forested ecosystems (e.g. Smith et al., 2009), the metric may not predict vegetation cover robustly in shrub-dominated ecosystems. The limited number of LiDAR returns from vegetation in shrub-dominated ecosystems likely results in an underestimation of cover calculated by Veg_Cov.

We found that our shrub cover predictive power increased at the 3 m spatial resolutiSon with the inclusion of both ARI2 and the red to green ratio (Table 3). The red to green ratio is a broadband vegetation index, which suggests that combing airborne LiDAR with information from multispectral sensors may also improve shrub cover estimation results. The selection of ARI2 and the red to green ratio highlights the importance of using vegetation indices related to the physiological status of shrubs to estimate cover. In addition, including spectral information decreased the RMSE. While this decrease was roughly 1% (Table 6), the contribution of spectral information may be significant when considering that shrub cover in our study area (median of 17.2-30.6% cover) and many areas in the Great Basin and other dryland systems is quite low. In addition, the photosynthetically active portion of many shrubs in the Great Basin (e.g. sagebrush) is small in comparison to the woody component (e.g. Olsoy et al., 2014). Due to the large spectral contribution of the woody component, narrow band indices are more likely to support retrieval of photosynthetic functional characteristics. Previous studies have also found narrow band indices helpful in characterizing dryland plants (e.g. Black & Guo, 2008; Lewis, 2002). Interestingly, vegetation indices associated with cellulose and lignin content, such as PSRI and NDII were not identified as important predictors of shrub cover. It is possible that the role of such indices were relatively minor compared to the larger contributions of LiDAR-derived variables. It should also be noted that the role of vegetation indices may change seasonally. For example, it may be easier to discriminate shrub woody biomass in the spring because cellulose and lignin indices would not be as sensitive to grasses greening up in comparison to senesced grass and litter in later summer and fall.

When LiDAR-only shrub cover was estimated for each site independently, individual sites had an r^2 ranging from 0.41 to 0.57. When all three sites were analyzed collectively, LiDAR-shrub cover estimation only had an r^2 value of 0.49. When HyMap / LiDAR shrub cover was estimated for each site independently, individual sites had an r^2 ranging from 0.52 to 0.65. By comparison, the HyMap / LiDAR cover estimation had an r^2 of 0.58 when all three sites were analyzed collectively. In all independent and collective site scenarios, combining the LiDAR variables with spectral variables improved correlation coefficients and reduced RMSE on the order of 1%. Analyzing the sites collectively resulted in correlation coefficients and RMSE values that were roughly an average of how each site performed independently. The RMSE behavior is difficult to predict if additional study sites were included in the analyses; however, it may prove helpful to developing a correction factor to account for consistent LiDAR shrub cover overestimation. It may also be that data fusion of LiDAR and spectral observations is key to constraining error when scaling from site-specific observations to a region in this open-canopy environment. Overall, these findings suggest that high quality field and airborne remote sensing datasets are necessary to estimate shrub cover at fine resolutions in the low-height, open canopy rangelands of the Great Basin.

Using a range of *in situ* data from the Great Basin, this study also demonstrated the potential of HyspIRI data to robustly estimate shrub cover and height. Studies such as the one presented herein help evaluate potential applications and vegetation products in anticipation of HyspIRI and other future space-borne imaging spectrometer missions. In this study, we were particularly interested in the capabilities of a sensor such as HyspIRI, with high spectral resolution and relatively coarse spatial resolution. Other hyperspectral and multispectral satellite missions such as Hyperion and Landsat 8 have unique challenges characterizing sparse, low-height vegetation in dryland systems (Jafari & Lewis, 2012). At the coarse scale, the strong relationship between mean vegetation height and HyspIRI-simulated indices related to red edge and anthocyanins is promising in terms of future satellite missions suitable for characterizing the effect of changes in ecosystem composition and function on resource management and 3-dimensional vegetation structure. Moreover, we found that HyspIRI-simulated variables related to the red edge, water content and anthocyanins, had high predictive power for both shrub cover and height. The shrub cover estimates provided by the HyspIRI-simulated variables are robust and the two methods to develop a spatially explicit dependent variable of shrub cover (imputation and point cloud data) provide a potential bounding range of error for HyspIRI (RMSE of 5 to 9%). In addition, predictions of height indicate that HyspIRI has the potential to also provide vertical structural metrics. The shrub cover estimated by the HyspIRI simulations did not capture the distribution of lower and upper shrub cover percentiles (minimum cover: 0 to 9%, maximum cover: 41.3 to 51.6 %; Table 5), which may be attributed to the effect of the coarser spatial resolution. The results show that while spectral range and resolution of HyspIRI are sufficient to capture the major range of shrub cover distribution, the coarser spatial resolution may become a key limitation to accurately recording the lower and upper ranges of shrub cover distribution (Figure 7). Methods for leveraging a greater range of spectral information should be investigated and additional methods and data should be used to create HypsIRI-simulated data for testing (NASA, 2013).

To improve upon this study at the fine scale, high fidelity hyperspectral and a narrower pulse width LiDAR (smaller beam diameter and shorter pulse length) will be needed to resolve low-height sparse vegetation. In addition, small footprint full-waveform LiDAR has not been demonstrated in dryland systems, mostly due to limited availability. While airborne LiDAR provides detailed structural metrics of vegetation, its large scale application to ecosystem analysis and modeling is limited by the lack of available data, and to some extent the variability in data quality and standards in which airborne LiDAR are collected. The challenges associated with availability may be mitigated by utilizing airborne LiDAR as a sampling tool, similar to in situ data collection (Wulder et al., 2012).

At the coarse scale, HyspIRI may be well complemented with structural measurements from satellite-based laser altimetry. While NASA's ICESat full-waveform GLAS instrument confounds energy peaks for rangeland vegetation and ground, resulting in a ground return pulse to widen from low vegetation (Duong et al., 2009; Hug et al., 2004), new potential may arise in the upcoming ICESat-2 mission. The photon counting instrument of ATLAS on ICESat-2 and operating with a green wavelength may not have the capacity to resolve low-height vegetation across fine scales, yet several mission characteristics have the potential to improve regional scale estimates of structural metrics (Yua et al., 2010). Current testing in shrub ecosystems using photon counting airborne MABEL (Multiple Altimeter Beam Experimental Lidar) data is underway.

Complimentary satellite-based high fidelity spectral and laser altimetry measurements will also enable improved physiological monitoring of shrublands. For example, linking estimates of leaf chemistry (e.g. N estimates in sagebrush, Mitchell et al., 2012) with shrub structural measurements will allow parameterization of shrublands in ecosystem models such as the Ecosystem Demography model (Antonarakis et al., 2014; Moorcroft et al., 2001). Synthesizing spatial predictions of vegetation parameters with remote sensing is critical for initialing models to estimate ecosystem fluxes. In sum, our results demonstrate the merit of coupling spectral and laser altimetry measurements for dryland shrub characterization. To leverage these synergistic data types, new methods are needed to optimize combination methods, address uncertainties associated with sensitivities to sampling size, understand relative tradeoffs and redundancies between sensors, and leverage the full range of hyperspectral information.

5. Acknowledgements

Research was funded by NOAA NA10OAR4680240, NASA NNX14AD81G, and with support from Idaho National Laboratory and USDA ARS Reynolds Creek Experimental Watershed.

6. References

Abrams, M., Pieri, D., Realmuto, V., & Wright, R. (2013). Using EO-1 Hyperion data as

HyspIRI preparatory data sets for volcanology applied to Mt Etna, Italy. *IEEE Journal of Selected Topics in Applied Earth Observations and Remote Sensing*, 6: 375 – 385. Doi: 10.1109/JSTARS.2012.2224095.

Anderson, J. E., & Inouye, R. S. (2001). Landscape-scale changes in plant species abundance and biodiversity of a sagebrush steppe over 45 years. *Ecological Monographs* 71, 531 – 556.

Anderson, J. E., Plourde, L. C., Martin, M. E., Braswell, B. H., Smith, M-L., Dubayah, R. O., Hofton, M. A. & Blair, J. B. (2008). Integrating waveform lidar with hyperspectral imagery for inventory of a northern temperate forest. *Remote Sensing of Environment* 112 (4), 1856 – 1870.

Antonarakis, A.S., Munger, J.W., & Moorcroft, P.R. (2014). Imaging spectroscopy- and lidar-derived estimates of canopy composition and structure to improve predictions of forest carbon fluxes and ecosystem dynamics, *Geophysical Research Letters* 41 7, 2535-2542.

Black, S. C., & Guo, X. (2008). Estimation of grassland CO exchange rates using hyperspectral remote sensing techniques. *International journal of remote sensing* 291, 145-155.

Breiman, L. (2001). Random forests. *Machine Learning*, 45, 5 − 32.

Breiman, L., Friedman, J.H., Olshen, R.A., & Stone, C.J. (1984). *Classification and Regression Trees* (pp. 121-125). New York: Chapman and Hall/CRC.

Castedo-Dorado, F., Gómez-Vázquez, I., Fernandes, P.M., & Crecente-Campo, F. (2012). Shrub fuel characteristics estimated from overstory variables in NW Spain pine stands, *Forest Ecology and Management*, 275, 130-141.

Ceccato, P., Flasse, S., Tarantola, S., Jacquemoud, S. & Gregoire, J.M. (2001). Detecting vegetation leaf water content using reflectance in the optical domain. *Remote Sensing of Environment 77*:22-33. 588

Claudio, H.C., Cheng, Y., Fuentes, D.A., Gamon, J. A., Luo, H., Oechel, W., Hong-Lie, Q., Rahman, A. F., & Sims, D. A., (2006). Monitoring drought effects on vegetation water content and fluxes in chaparral with the 970 nm water band index. *Remote Sensing of Environment*, 103, 304 – 311.

Cocks, T., Jenssen, R., Stewart, A., Wilson, I., & Shields, T. (1989). The HyMap airborne hyperspectral sensor: the system, calibration and performance. In: Schaepman, M. E., Schlaepfer, D. & Itten, K. I. (Eds.), Proceedings of the First EARSeL Workshop on Imaging Spectroscopy. EARSeL, Zürich, Switzerland p 37–42.

Crawford, J.A., Olson, R. A., West, N.E., Mosley, J.C., Schroeder, M.A., Whitson, T.D., Miller, R.F., Gregg, M.A., & Boyd, C. S. (2004). Ecology and management of sage-grouse and sage-grouse habitat. *Journal of Range Management*, 57, 2 – 19.

Crookston, N.L., & Finley, A.O. (2008). yaImpute: An R package for kNN imputation. *Journal of Statistical Software*, 23, 1 – 16.

Curran, P.J., Windham, W.R., & Gholz, H.L. (1995). Exploring the Relationship between Reflectance Red Edge and Chlorophyll Concentration in Slash Pine Leaves. *Tree Physiology* 15, 203 – 206.

Díaz-Uriarte, R., & Alvarez de Andrées, S. (2006). Gene Selection and classification of microarray data using random forest. *BMC Bioinformatics*, 7, 3.

Dixit, L. & Ram, S. (1985).Quantitative analysis by derivative electronic spectroscopy. *Applied Spectroscopy Reviews*., 21, 311 – 418.

Duong, H., Lindenbergh, R., Pfeifer, N., & Vosselman, G. (2009). ICESat full-waveform altimetry compared to airborne laser scanning altimetry over the Netherlands. IEEE Transactions on Geoscience and Remote Sensing, 47(11), 3365 – 3378.

Esteban, J., Starr, A., Willetts, R., Hannah, P., & Bryanston-Cross, P. (2005). A review of data fusion models and architectures: towards engineering guidelines. *Neural Computing & Applications*, 14: 273 – 281.

Falkowski, M. J., Hudak, A. T., Crookston, N. L., Gessler, P. E., Uebler, E. H., & Smith, A. M. (2010). Landscape-scale parameterization of a tree-level forest growth model: a k-nearest neighbor imputation approach incorporating LiDAR data. *Canadian Journal of Forest Research*, *40,* 184 – 199.

Gamon, J. A. & Surfus, J. S. (1999). Assessing leaf pigment content and activity with a reflectometer. *New Phytologist, 143*, 105 – 117.

Gamon, J. A., Serrano, L. & Surfus, J. S. (1997). The Photochemical Reflectance Index: An Optical Indicator of Photosynthetic Radiation Use Efficiency across Species, Functional Types and Nutrient Levels. *Oecologia 112*, 492 – 501.

Gao, B., & Goetz, A. F. H. (1990). Column atmospheric water vapor and vegetation liquid water retrievals from airborne imaging spectrometer data. *Journal Geophysical Research*, *95,* 3549 – 3564.

Gao, B.C., Heidebrecht, K.B., & Goetz, A.F.H. (1992). ATmospheric REMoval Program (ATREM) User's Guide, Center for the Study of Earth from Space document, version 1.1. University of Colorado, 24 pp.

Gislason, P. O., Benediktsson, J. A., & Sveinsson, J. R. (2006). Random Forests for land cover classification. *Pattern Recognition Letters, 27*, 294-300.

Gitelson, A. A., & Merzlyak, M. N. (1996). Signature analysis of leaf reflectance spectra: algorithm development for remote sensing of chlorophyll. *Journal of Plant Physiology*, *148*, 494 – 500.

Gitelson, A.A. & Merzlyak, M. N. (1994). Spectral reflectance changes associated with autumn senescence of *Aesculus Hippocastanum* L. and *Acer Platanoides* L. leaves. Spectral features and relation to chlorophyll estimation. *Journal of Plant Physiology*143:286-292.

Gitelson, A.A., Y. Zur, O.B. Chivkunova, & Merzlyak, M.N. (2002). Assessing carotenoid content in plant leaves with reflectance spectroscopy. *Photochemistry and Photobiology* 75:272-281.

Gitelson, A.A., Merzlyak, M.N. & Chivkunova, O.B. (2001). Optical properties and nondestructive estimation of anthocyanin content in plant leaves. *Photochemistry and Photobiology*, 71, 38 – 45.

Gitelson, A. A., Kaufman, Y.J., & Merzlyak, M. N. (1996). Use of a green channel in remote sensing of global vegetation from EOS-MODIS. *Remote Sensing of Environment*, 58, 289 – 298.

Glenn. N., Spaete, L., Sankey, T., & Mitchell, J. (2011). Errors in LiDAR-derived shrub height and crown area on sloped terrain, *Journal of Arid Environments*, 75 (4), 377 –382.

Greig-Smith, P. (1983). Quantitative Plant Ecology, Berkeley: University of California Press.

Guo, L, Chehata, N., Mallet, C., & Boukir, S. (2011). Relevance of airborne lidar and multispectral image data for urban scene classification using Random Forests, *ISPRS Journal of Photogrammetry and Remote Sensing*, 66 (1), 56 – 66.

Hardisky, M.A., Klemas, V. & Smart, R.M. (1983). The influences of soil salinity, growth form, and leaf moisture on the spectral reflectance of *Spartina alterniflora* canopies. *Photogrammetric Engineering and Remote Sensing*, 49, 77 – 83.

Homer, C. G., Aldridge, C. L., Meyer, D. K., & Schell, S. J. (2012). Multi-scale remote sensing sagebrush characterization with regression trees over Wyoming, USA: Laying a foundation for monitoring. *International Journal of Applied Earth Observation and Geoinformation,* 14, 233 – 244.

Hudak, A. T., Crookston, N. L., Evans, J. S., Hall, D. E., & Falkowski, M. J. (2008). Nearest neighbor imputation of species-level, plot-scale forest structure attributes from LiDAR data. *Remote Sensing of Environment*, 112, 2232 − 2245.

Huete, A.R., Liu, H., Batchily, K & van Leeuwen, W. (1997). A comparison of vegetation indices over a global set of TM images for EOS-MODIS. *Remote Sensing of Environment* 59(3):440-451.

Hug, C., Ullrich, A., & Grimm, A. (2004). Litemapper-5600-a waveform-digitizing LiDAR terrain and vegetation mapping system. *International Archives of Photogrammetry, Remote Sensing and Spatial Information Sciences, 36*(Part 8), W2.

Hunt Jr., E.R. & Rock, B.N. (1989). Detection of changes in leaf water content using near- and middle-infrared reflectances. *Remote Sensing of Environment* 30:43-54.

Jafari, R. & Lewis, M.M. (2012). Arid land characterization with EO-1 Hyperion hyperspectral data, *International Journal of Applied Earth Observation and Geoinformation*, 19, 298 – 307.

Keane, R. E., Rollins, M. G., McNicoll, C. H., & Parsons, R. A. (2002). Integrating ecosystem sampling, gradient modeling, remote sensing, and ecosystem simulation to create spatially explicit landscape inventories. RMRS-GTR-92. U.S. Department of Agriculture, Fort Collins, CO, Forest Service, Rocky Mountain Research Station. 61 pp.

Knick, S. T., & Connelly, J. W. (2009). Greater sage-grouse and sagebrush: an introduction to the landscape. Studies in Avian Biology. In press. Page 14 of .pdf available at: http://sagemap.wr.usgs.gov/Docs/SAB/Chapter01.pdf.

Krogh, S. N., Zeisset, M. S., Jackson, E., & Whitford, W. G. (2002). Presence/absence of a keystone species as an indicator of rangeland health. *Journal of Arid Environments*, 50(3), 513 – 519.

Kruse, F. A., Taranik, J. V., Coolbaugh, M., Michaels, J., Littlefield, E. F., Calvin, W. M., & Martini, B. A. (2011). Effect of reduced spatial resolution on mineral mapping using imaging spectrometry—examples using Hyperspectral Infrared Imager (HyspIRI)-simulated data. *Remote Sensing*, 3(8), 1584 – 1602.

Laliberte, A. S., Fredrickson, E. L., & Rango, A. (2007). Combining decision trees with hierarchical object-oriented image analysis for mapping arid rangelands. *Photogrammetric Engineering and Remote Sensing*, 73(2): 197 – 207.

Latifi, H., Fassnacht, F. & Koch, B. (2012). Forest structure modeling with combined airborne hyperspectral and LiDAR data, *Remote Sensing of Environment*, 121, 10 –25.

Lee, J. H., Timmermans, J., Su, Z., & Mancini, M. (2012). Calibration of aerodynamic roughness over the Tibetan Plateau with Ensemble Kalman Filter analysed heat flux. *Hydrology & Earth System Sciences*, 16, 4291 – 4302. Doi:10.5194/hess-16-4291-2012.

Leutner, B.F., Reineking, B., Müller, J., Bachmann, M., Beierkuhnlein, C., Dech, S., Wegmann, M. (2012). Modelling Forest α-Diversity and Floristic Composition — On the Added Value of LiDAR plus Hyperspectral Remote Sensing. *Remote Sensing*, 4, 2818 – 2845.

Lewis, M.M., (2002). Spectral characterization of Australian arid zone plants, *Canadian Journal of Remote Sensing*, 28 (2):219-230.

Lobell, D.B. & Asner, G.P. (2003). Hyperion studies of crop stress in Mexico. *Proceedings of the 12th Annual JPL Airborne Earth Science Workshop*. Pasadena, CA. Retrieved from ftp://popo.jpl.nasa.gov/pub/docs/workshops/03_docs/lobell_aviris_2003_web.pdf on 01 April, 2015.

Mathieu, R., Naidoo, L., Cho, M., Leblon, B., Main, R., Wessels, K., Asner, G., Buckley, J., Van Aardt, J., Erasmus, B., & Smith, I. (2013). Toward structural assessment of semi-arid African savannahs and woodlands: The potential of multitemporal polarimetric RADARSAT-2 fine beam images, *Remote Sensing of Environment*, 138, 215 – 231.

Medvigy, D., Wofsy, S., Munger, J., Hollinger, D., & Moorcroft, P. (2009). Mechanistic scaling of ecosystem function and dynamics in space and time: Ecosystem Demography model version 2. Journal of Geophysical Research: Biogeosciences (2005–2012), 114

Merzlyak, J. R., Gitelson, A. A., Chivkunova, O.B. & Rakitin, V.Y. (1999). Non-destructive optical detection of pigment changes during leaf senescence and fruit ripening. *Physiologia Plantarum* 106:135-141.

Mitchell, J., Moore, C., & Glenn, N. (2013). Single and multi-date Landsat classifications of basalt to support Soil Survey efforts, *Remote Sensing*, 5(10), 4857 – 4899.

Mitchell, J., Glenn, N. F., Sankey, T., Derryberry, D. R., & Germino, M. (2012). Remote sensing of sagebrush canopy nitrogen, *Remote Sensing of Environment*, 124, 217-223.

Mitchell, J., Glenn, N., Sankey, T., Derryberry, D., Anderson, M. & Hruska, R. (2011). Sagebrush canopy height and shape estimations using small footprint LiDAR, *Photogrammetric Engineering and Remote Sensing*, 77 (5), 521 – 530.

Mitchell, J., and Glenn, N. F. (2009). Leafy Spurge (*Euphorbia esula* L.) classification performance using hyperspectral and multispectral sensors. *Rangeland Ecology and Management*, 62: 16 – 27.

Moorcroft, P., Hurtt, G., & Pacala, S.W. (2001). A method for scaling vegetation dynamics: the ecosystem demography model (ED). Ecological Monographs, 71, 557-586.

Mueller, E. N., Wainwright, J. & Parsons, A. J. (2007). Impact of connectivity on the modeling of overland flow within semiarid shrubland environments. *Water Resources Research* 43.

Mundt, J., Streutker, D. & Glenn, N. (2006). Mapping sagebrush distribution using fusion of hyperspectral and lidar classifications. *Photogrammetric Engineering & Remote Sensing*, 72 (1): 47 – 54.

National Aeronautics and Space Administration (NASA) (2014). HyspIRI mission study. NASA Jet Propulsion Laboratory. http://hyspiri.jpl.nasa.gov/

National Aeronautics and Space Administration (NASA) (2013). HyspIRI 2013 Workshop Agenda. NASA Jet Propulsion Laboratory. http://hyspiri.jpl.nasa.gov/documents/2013-workshop.

National Research Council. Committee on Earth Science and Applications from Space (2007). *Earth science and applications from space: National imperatives for the next decade and Beyond* (456 pp.). Washington, D. C.: National Academies Press.

Okin, G. S., Roberts, D. A., Murray, B. & Okin, W. J. (2001). Practical limits on hyperspectral vegetation discrimination in arid and semiarid environments. *Remote Sensing of Environment*, 77, 212 – 215.

Okin, G. S. (2008). A new model of wind erosion in the presence of vegetation. *Journal of Geophysical Research: Earth Surface (2003–2012)*, *113*(F2).

Olsoy, P., Glenn, N., Clark, P., & Derryberry, D. (2014). Aboveground total and green biomass of dryland shrub derived from terrestrial laser scanning. *ISPRS Journal of Photogrammetry and Remote Sensing*, 88, 166 – 173.

Olsson, A. D., & Morisette, J. T. (2014). Comparison of Simulated HyspIRI with Two Multispectral Sensors for Invasive Species Mapping. *Photogrammetric Engineering & Remote Sensing*, 80(3), 217 – 227.

Pal, M. (2005). Random forest classifier for remote sensing classification. *International Journal of Remote Sensing*, *26*, 217 – 222.

Pearlman, J. S., Barry, P. S., Segal, C. C., Shepanski, J., Beiso, D., & Carman, S. L. (2003). Hyperion, a space-based imaging spectrometer. *Geoscience and Remote Sensing, IEEE Transactions on*, 41(6), 1160 – 1173.

Peñuelas, J., Pinol, J., Ogaya, R. & Filella, R. (1997). Estimation of plant water concentration by the reflectance water index WI (R900/R970)

Purevdorj TS, Tateishi R, Ishiyama T, & Honda, Y. (1998). Relationships between percent vegetation cover and vegetation indices. *International Journal of Remote Sensing* 19: 3519 – 3535.

Ramsey, R.D., Wright Jr., D.L. & McGinty, C. (2004). Evaluating the use of Landsat 30m Enhanced Thematic Mapper to monitor vegetation cover in shrub-steppe environments. *Geocarto International*, 19:39 – 47.

Roberts, D.A., Quattrochi, D.A., Hulley, G.C., Hook, S.J. & Green, R.O. (2012) Synergies between VSWIR and TIR data for the urban environment: An evaluation of the potential for the Hyperspectral Infrared Imager (HyspIRI) Decadal Survey mission, *Remote Sensing of Environment*, 117: 83 – 101.

Rodriguez-Galiano, V. F., Ghimire, B., Rogan, J., Chica-Olmo, M., & Rigol-Sanchez, J. P. (2012). An assessment of the effectiveness of a random forest classifier for land-cover classification. *ISPRS Journal of Photogrammetry and Remote Sensing*, 67: 93 – 104.

Rouse, J. W., Haas, R. H., Schell, J. A., & Deering, D. W. (1973). Monitoring vegetation systems in the great plains with ERTS, in *Third ERTS Symposium*, NASA SP-351, NASA, Washington, DC, Vol. 1, p. 309 – 317

Schlesinger, W. H., Reynolds, J. F., Cunningham, G. L. , Huenneke, L. F., Jarrell, W. M., Virginia, R. A. & Whitford, W. G. (1990). Biological Feedbacks in Global Desertification, *Science*, 247: 1043 – 1048, doi: 10.1126/science.247.4946.1043.

Serrano, L., Penuelas, J. & Ustin, S.L. (2002). Remote Sensing of Nitrogen and Lignin in Mediterranean Vegetation from AVIRIS Data: Decomposing Biochemical from Structural Signals. *Remote Sensing of Environment* 81:355 – 364.

Sims, D.A. & Gamon, J.A. (2002). Relationships Between Leaf Pigment Content and Spectral Reflectance Across a Wide Range of Species, Leaf Structures and Developmental Stages. *Remote Sensing of Environment* 81:337 – 354.

Sivanpallai, R., Prager, S. D., & Storet, T. O. (2009). Estimating sagebrush cover in semi-arid environments using Landsat Thematic Mapper data. . *International Journal of Applied. Earth Observation and Geoinformation,* 11, 103 – 107.

Smith, A. M., Falkowski, M. J., Hudak, A. T., Evans, J. S., Robinson, A. P., & Steele, C. M. (2009). A cross-comparison of field, spectral, and lidar estimates of forest canopy cover. *Canadian Journal of Remote Sensing*, 35(5), 447-459.

Smith, M.O., Ustin, S.L., Adams, J.B. & Gillespie, A.R. (1990). Vegetation in deserts: I. A regional measure of abundance from multispectral images. *Remote Sensing of Environment*, 31(1), 1 – 26.

Spaete, L., Glenn, N., Derryberry, D., Sankey, T., Mitchell, J & Hardegree S. (2011). Vegetation and slope effects on accuracy of a LiDAR-derived DEM in the sagebrush steppe. *Remote Sensing Letters*, 2 (4): 317 – 326.

Stow, D., Hamada, Y., Coulter, L., & Anguelova, Z. (2008). Monitoring shrubland habitat changes through object-based change identification with airborne multispectral imagery.

Remote Sensing of Environment, 112(3), 1051 – 1061.

Streutker, D. & Glenn, N. (2006). LiDAR measurement of sagebrush steppe vegetation heights, *Remote Sensing of Environment*, 102 (1): 135 – 145.

Streutker, D., Glenn, N. & Shrestha, R. (2011). A slope-based method for matching elevation surfaces. *Photogrammetric Engineering & Remote Sensing*, 77 (7):743 –750.

Strobl, C., Malley, J., & Tutz, G. (2009). An introduction to recursive partitioning: rationale, application,and characterisitics of classification and regression trees, bagging, and random forests. *Psychological Methods*, 14(4): 323 – 348.

Suring, L.H., Rowland, M.M., & Wisdom, M.J. (2005). Identifying species of conservation concern. *In*: Wisdom MJ, Rowland MM, Suring LL, editors. Habitat threats in the sagebrush ecosystem: methods of regional assessment and applications in the Great Basin. Lawrence, KS: Alliance Communications Group, pp. 150–162

Swatantran, A., Dubayah, R., Roberts, D., Hofton, J. & Blair. (2011). Mapping biomass and stress in the Sierra Nevada using lidar and hyperspectral, *Remote Sensing of Environment*, *211*, 2917 – 2930.

Tilley, D., D., Ogle, L. St John, & Benson, B. (2006). Plant Guide for Big Sagebrush (*Artemisia tridentata*). USDA-Natural Resources Conservation Service Idaho Plant Materials Center.

Tucker, C.J., (1979). Red and Photographic Infrared Linear Combinations for Monitoring Vegetation. Remote Sensing of the Environment 8:127-150.

USDA ARS Northwest Watershed Research Center (2014), 'reynolds-creek-098c-annual-precipitation.dat'. Retrieved from ftp://ftp.nwrc.ars.usda.gov/publicdatabase/ on 21 February, 2015.

Vauhkonen, J., (2010). Imputation of single-tree attributes using airborne laser scanning-based height, intensity, and alpha shape metrics. *Remote Sensing of Environment* 114: 1263 – 1276.

Vogelmann, J.E., Rock, B. N. & Moss, D. M. (1993). Red Edge Spectral Measurements from Sugar Maple Leaves. *International Journal of Remote Sensing* 14: 1563 – 1575.

Wulder, M.A., White, J.C., Bater, C.W., Coops, N.C., Hopkinson, C. & Chen, G. (2012). Lidar plots—a new large-area data collection option: context, concepts, and case study. *Canadian Journal of Remote Sensing* 38: 600 – 618.

Yua, A.W., Stephen, M.A., Li, S.X., Shaw, G.B., Seas, A., Dowdye, E., Troupaki, E., Liiva, P., Poulios, D., Mascetti, K. (2010). Space Laser Transmitter Development for ICESat-2 Mission, *Proc. of SPIE*, Vol. 7578 757809.

Zeng, X., Zeng, X., & Barlage, M. (2008). Growing temperate shrubs over arid and semiarid regions in the Community Land Model–Dynamic Global Vegetation Model. Global Biogeochemical Cycles, 22, GB3003.

Zhang, Q., Middleton, E. M., Gao, B. C., & Cheng, Y. B. (2012). Using EO-1 hyperion to simulate HyspIRI products for a coniferous forest: The fraction of PAR absorbed by chlorophyll and leaf water content (LWC). *IEEE Transactions on Geoscience and Remote Sensing*, 50(5), 1844 – 1852.

Zolkos, S.G., Goetz, S.J., & Dubayah, R. (2013). A meta-analysis of terrestrial aboveground biomass estimation using lidar remote sensing. *Remote Sensing of Environment*, *128*, 289 – 298